Frequency-Dependent Permeability Evaluation by Harmonic Resonance Cavity Perturbation Method

Taro Miura, *Life Member, IEEE*, and Ken Tahara, *Member, IEEE*

***Abstract*— An artificial material made by kneading magnetic metal flakes in plastic sheets has been used widely in PCs or mobile phone handsets. This sheet is called a noise suppression sheet to reduce unwanted coupling or unwanted signals in the device. The sheet has strong frequency-dependent characteristics in the permeability. It is essential to evaluate these characteristics accurately to develop the sheets and to design the device mentioned above. Currently, the sheets have been evaluated by the transmission line methods, but the accuracy was not enough. The evaluation by the resonance cavity perturbation method is proposed in this article. Although the accuracy of the resonance cavity perturbation method is high, it works well at only one resonance frequency. The expansion of the measuring frequency by using a harmonic resonance cavity is proposed in this article. A comparison of the proposed method to the transmission line method is also discussed.**

***Index Terms*— Cavity perturbation methods, frequency characteristics, permeability, resonators, waveguide components.**

I. Introduction

RECENTLY, artificial materials made by kneading magnetic metal flakes in plastic sheets have been widely used in PCs or mobile phone handsets. This sheet is well known as a noise suppression sheet (NSS) and is used to reduce unwanted signals in transmission lines or unwanted couplings between circuit elements in the devices described above. It has been considered that the structure of the sheet would bring strong frequency-dependent characteristics and anisotropy. The accurate characterization of the sheet becomes essential to the development of the sheet, as well as to the design of the circuit boards for PCs and mobile phone handsets by electromagnetic structure simulations.

The Nicolson–Ross–Weir (NRW) method has been used widely for the characterization of the NSS [1], [2]. This method evaluates the characteristics of the S-parameters of a transmission line installing the NSS. This method could give the permeability and the permittivity of a sample simultaneously among the broad frequency range. A short evaluation time has also been the advantage of this method.

However, in some cases, the complicated calculation process from the network analyzer data to the physical quantities can lead to ambiguities and unrealistic results and uncertain reliability. The permeability evaluation of the NSS by a shorted transmission line with a small piece of the sample has been another popular method [3]–[5]. The very simple structure of the test fixture made it easy to evaluate the permeability of the material, and continuous evaluation over the frequency range is the advantage of the method. However, two problems concerning this method were considered. One problem is the requirement for the excellent impedance matching between the connector and the test fixture for broadband measurements. Unwanted reflection from the connecting point would harm the accuracy, and it is very difficult to separate the contribution of the reflection from the obtained data. The other problem is the determination of the depolarization factor of the test sample. The depolarization factor depends on the permeability, and the shape of the sample would make it difficult to obtain accurate results. It is well known that only an isotropic spheroid has an analytical solution and other shapes have approximated values.

The resonance cavity perturbation method is a classical method, and it enables the permeability and the permittivity evaluation over a broad frequency range using the same sample in the range of different cavities of different resonance frequencies. When a small sample is put into a region of strongest magnetic field strength and zero electric field strength parts of a cavity, the resonance frequency shifts proportional to the permeability of the material, and the cavity loss factor increases with the loss of the material. The perturbation evaluated in the cavity with a small coupling factor means that the connection to the outside would have a small influence on the results. Regarding the evaluation of material characteristics by the resonance cavity perturbation method, a demagnetizing or a depolarizing field appears at both ends of the sample, and the field changes the permeability or the permittivity given by measurements. The estimation by the demagnetization or depolarization becomes essential in the evaluation procedure, and this will be discussed in this article.

In the evaluation of the permeability by the resonance cavity perturbation method, a thin disk has been used as a sample [6]. A thin stick longer than the cavity height will be used as a sample in this article. The stick is installed in the cavity where the magnetic flux density is null, and the evaluation could be made by ignoring the demagnetization. This is an advantage of this method. A good conductor shows the permeability of null at the microwave frequency range. This means that the conductor becomes a reference material to define the proportional constant of the cavity with the relative permeability of 1 given by the air. The calibration of the cavity

Manuscript received July 7, 2019; revised November 14, 2019 and December 22, 2019; accepted January 13, 2020. *(Corresponding author: Taro Miura.)*

Taro Miura is with The Mueller Consultant, Tokyo 168-0081, Japan (e-mail: tmuller.com@tech.email.ne.jp).

Ken Tahara is with KEN-TEC Corporation, Tokyo 186-0011, Japan (e-mail: ktahara@peace.ocn.ne.jp).

Color versions of one or more of the figures in this article are available online at http://ieeexplore.ieee.org.

Digital Object Identifier 10.1109/TMTT.2020.2974841

using the good conductor could give consistent solutions, and this is the other advantage of the permeability evaluation by the resonance cavity perturbation method [7].

The resonance cavity perturbation method has been more popular to evaluate the permittivity of a sample than to evaluate the permeability. For the permittivity, the sample is positioned in a region of the strongest electric field and zero magnetic field strengths within the cavity. The proportional constant in the evaluation of the permittivity is 2 [6]. However, an electric field not parallel to the sample appears around the sample insertion hole of the cavity, and the field becomes a depolarization field. This means that the electromagnetic circumstance is clearly different from the evaluation of the permeability. The analysis of the depolarization becomes essential to obtain accurate results. Many articles have been published to solve this [8] and [9], but the rigorous solution to give the depolarization has not been given yet. Therefore, the evaluation of the permeability is clearly different from the evaluation of the permittivity, and the procedure to obtain accurate permittivity would contribute little to the improvement of the permeability evaluation.

A rectangular waveguide shorted at both ends will resonate at those frequencies for which the length is equal to an integral multiple of a half wavelength in the waveguide. If only single mode, such as TE_{10}, is found in the waveguide, this can be called a harmonic resonance cavity because the resonance will be observed at the harmonic number, n, of the waveguide mode. It is proposed here to use the resonator to evaluate the frequency characteristics of materials by the resonance cavity perturbation method. An earlier article [10] used a TE_{10n} rectangular waveguide as the harmonic resonator to evaluate the permittivity in X-band, and the obtained data were used to increase the measuring accuracy. An expansion of the method to the broadband evaluation of the permeability was proposed earlier [11]. The frequency-dependent characteristics of the magnetic materials in the microwave frequency range obtained by the single resonance frequency cavity to the harmonic resonance frequency cavity perturbation method will be discussed in this article.

First, the principle of the cavity resonance perturbation method and the harmonic resonance of the rectangular waveguide cavity will be reviewed briefly. The design concept of the rectangular waveguide cavity for a broadband operation and the cavities assembled by applying the design concepts will be discussed next. The permeability evaluation of the materials by the harmonic resonance cavity perturbation (HRCP) method with the calibration method will be discussed in Section III. The permeability evaluation from the microwave frequency range to the UHF band will be made in this section. Finally, the confirmation of the measured results will be made based on the characteristics evaluation of an NSS in the actual transmission line.

II. Resonance Cavity Perturbation Method

An exchange between magnetic and electric energies occurs after an electromagnetic stimulus is given from a small aperture to a metal closed cavity. This is called the natural resonance, and the resonance will be decreased by the cavity wall energy loss. If the stimulus is applied with the same interval as the energy exchange, the energy in the cavity increases until the energy loss in the cavity becomes the same as the external energy supplied. This is called the electromagnetic resonance. The electric field strength in the cavity is null where the magnetic field strength is the maximum and vice versa. A material installed in the magnetic field maximum part shifts the resonance characteristics in proportion to the magnetic characteristics. A small sample in the cavity gives a fractional change in the resonance frequency, as shown in the following equation:

$$\frac{\Delta\omega}{\omega_0} = -\frac{\Delta W}{W_0} \tag{1}$$

where $\Delta\omega$ is the shift in the resonance frequency ω_0 and ΔW is the change in the stored energy W_0.

The electromagnetic expression of the above terms are shown in the following:

$$\Delta W = \frac{1}{2}\int_{\Delta v} (\varepsilon_0\varepsilon_{\mathrm{r}} E \cdot E^* + \mu_0\mu_{\mathrm{r}} h \cdot h^*) dV \tag{2}$$

where ε_0 is the permittivity of vacuum, μ_0 is the permeability of vacuum, ε_{r} is the relative permittivity of the material, and μ_{r} is the relative permeability of the material. The asterisk shows the complex conjugate of the field vector. The integration is over the volume of the sample. The stored energy W_0 is described as follows:

$$W_0 = \frac{1}{2}\int_{V} (\varepsilon_0 E \cdot E^* + \mu_0 h \cdot h^*) dV \tag{3}$$

where the integral is over the volume of the cavity.

If the sample is small and located at the region of the maximum of $\boldsymbol{h}$ in the cavity, the energy change, ΔW in the cavity is proportional to the permeability of the sample. The method to characterize the material, as shown above, is called the resonance cavity perturbation method. The permeability of the sample is written as in the following equation:

$$\mu_{\mathrm{r}}' - j\mu_{\mathrm{r}}'' = 1 + \frac{V}{\alpha_m \Delta v}\left[\frac{\Delta\omega}{\omega} - j\frac{1}{2}\left(\frac{1}{Q_s} - \frac{1}{Q_0}\right)\right] \tag{4}$$

where α_m is the factor defined by the sample position and the cavity mode, Q is the Q-factor of the cavity, and the suffixes s and 0 means that the cavity state shows whether the sample position is installed or vacant.

The equation shows that the real part of the material constant is described by the resonance frequency shift ratio, and the imaginary part is described by the increase of the cavity loss. A clear one-to-one relationship between the frequency shift ratio and the loss increase to the permeability is confirmed by the equation. The equation above shows that the accuracy of the resonator characteristics is essential to evaluate the permeability. The resonance frequency of the resonator is given by the average of the two frequencies showing the half value of the peak power in the resonance curve. The standard deviation of the resonance frequency was less than 0.1 parts per million (ppm) of the resonance frequency, and the accuracy is enough for this measurement. The loss factor of the resonator, $1/Q$, was evaluated from the area of the resonance curve using the resonance curve area method. The standard

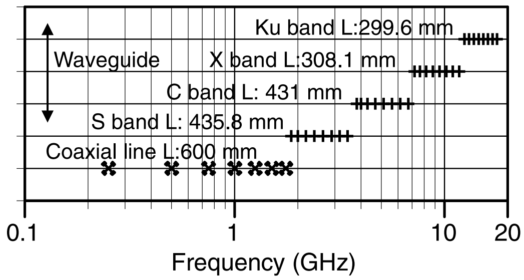

Fig. 1. Examples of resonance frequencies of resonators.

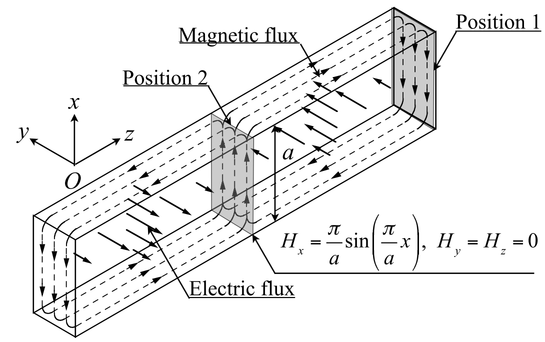

$$H_x = \frac{\pi}{a}\sin\left(\frac{\pi}{a}x\right),\ H_y = H_z = 0$$

Fig. 2. Example of the electromagnetic flux to evaluate permeability in the harmonic resonance cavity resonator.

deviation of the Q-factor evaluated by this method was less than 0.02% of the Q-factor, and the data dispersion of this method was one order smaller than the circle fitting method installed in the network analyzer [12].

The resonators operating in the coaxial TEM-mode line and the $\mathrm{TE_{10n}}$-mode rectangular waveguide are selected as the resonance cavity because the modes are the dominant mode of the waveguides and lines. They have a broad single-mode frequency range until the next higher modes appear. The resonance frequencies of the TEM-mode coaxial line resonator and the $\mathrm{TE_{10n}}$-mode rectangular waveguide resonator with the wavenumbers in the line are given as shown in the following equations, respectively:

$$F_{\mathrm{r}}(n) = 150\frac{n}{L} \tag{5}$$

$$F_{\mathrm{r}}(n) = 150\sqrt{\frac{1}{W^2} + \frac{n^2}{L^2}} \tag{6}$$

where n is the wavenumber in the cavity, L is the cavity length, and W is the width of the waveguide in mm.

The resonators to satisfy (5) or (6) have the continuous integral wavenumbers in the resonator, and they could be called the harmonic resonator. Examples of the resonance frequencies of the TEM coaxial line and the rectangular waveguides with the band name of IEC are shown in Fig. 1.

The resonance frequency interval of the coaxial line is arithmetic, and the resonance frequency intervals of the waveguides are approximately geometric. Fig. 1 shows that the waveguide resonators were suitable to know the profile of the material characteristics with appropriate frequency intervals.

A proposal to use the harmonic resonator for the resonance cavity perturbation method was discussed to evaluate the frequency-dependent characteristic of materials. An example of the electromagnetic flux distribution in the waveguide to evaluate the permeability is shown in Fig. 2. For the cavity resonator operated in the even mode number, the magnetic flux density is the maximum, and no electric flux is found at both ends, Position 1, and at the center, Position 2, of the resonator.

When the sample is installed at the parts described above, the resonance characteristics would be changed according to the magnetic characteristics of the sample.

A. Harmonic Resonance Cavity for Perturbation Method

The $\mathrm{TE_{10n}}$ modes of a rectangular waveguide resonator were considered first because the material characterization lower than 1 GHz has already been established by using network analyzers and test fixtures for this use. Currently, the frequency range was extended to 2 GHz by reducing the accuracy. The waveguide resonator would be suitable for the cavity perturbation method for higher than 2 GHz considering the dimension of the waveguide cavity. As discussed earlier, the characterization of the material is carried out only at the resonance frequency of the cavity. The shorter resonance frequency interval could give precise characteristics, but too narrow at interval needs a long cavity length and would cause the resonance peak interaction between the adjacent resonance peaks. The resonance frequency interval is decreased with the cavity length, as shown in (6). Eight resonance frequencies in a band were defined at the first step. A pair of loop antennas is used to launch and to detect the cavity power. A unidirectional magnetic field generated by the loop antenna would be appropriate to use the cavity under the defined mode. A low impedance of the loop antenna could protect the measuring equipment from an accidental electrical shock.

Two sample positions, at the end and at the center of the cavity, were considered for the permeability measurement, as shown in Fig. 2 for the case of $n = 2$. In the measurement of the permeability, the position at the end of the cavity could be used for all resonance mode numbers, and the position at the center of the cavity could be used for even resonance modes. The measurement at the end of the cavity reduces the cavity length to the minimum. However, a small shift of the sample position from the maximum magnetic field strength, position 1 in Fig. 2, caused by the sample thickness would reduce the accuracy. The measurement at the center of the cavity improves the accuracy because the center of the sample coincides with the maximum magnetic field, but the choice of the position increases the cavity length twice to the position 1 if the measuring frequency intervals are the same. The position 1 was used only for the measurement of lower frequency band because the sample position shift would be small to the wavelength in the cavity, and the cavity length could be reduced. Other positions to satisfy the permeability evaluation could be found in the cavity, but these positions reduce the number of measuring frequencies within the limited cavity length.

The coupling factor of the cavity increases with the resonance frequency increase of the loop antenna impedance and the Q-factor of the resonator with frequency. The resonance

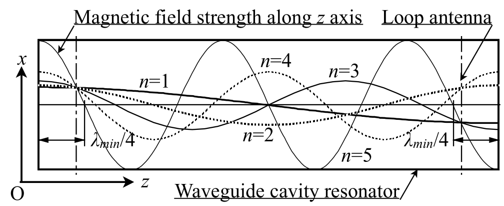

Fig. 3. Basic idea to maintain the coupling factor change small (λ min: length of highest resonance frequency wave).

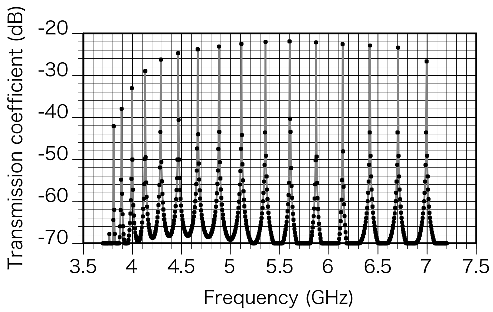

Fig. 4. Optimized transmission characteristics given by simulation.

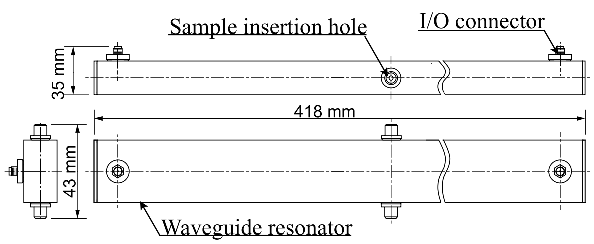

Fig. 5. Structure of C-band rectangular waveguide cavity (the longer side of the resonator is cut away to show whole).

cavity perturbation method evaluates the material characteristics by the changes of the resonance characteristics in the cavity isolated from the external circuit. A tight coupling between the cavity and the external circuit would reduce the accuracy. It would be favorable to maintain the coupling factor of the cavity less than -20 dB within the broad measuring frequency range. This has been established by defining the generating and detecting loop antenna positions very close to the minimum magnetic field position at the highest resonance frequency. The idea of this structure is shown in Fig. 3.

The definition of the loop antenna positions by RF transmission theory is very complicated. An RF structural simulator was used to optimize the generating and detecting loop antenna positions. The result of the simulation with Femtet_Ver_6 for the cavity in the C band is shown in Fig. 4, as an example.

The top view, the plane, and the side view of the cavity used in the simulation are illustrated in Fig. 5 by a technical drawing.

The magnetic field strength at the center of the C-band cavity around the sample installing area is shown in Fig. 6.

Fig. 6 shows that the magnetic field strength H_x, at the center of sample area is the maximum and 0 at the top and the bottom of the cavity, as shown in Fig. 6. This means that the demagnetization field is 0 at both ends of the sample.

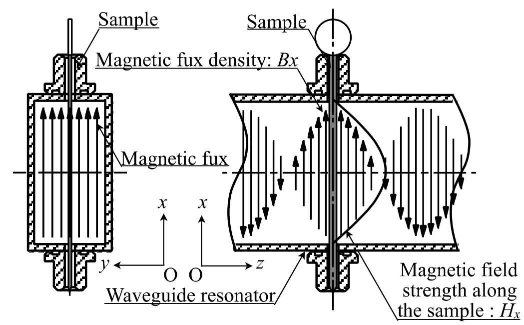

Fig. 6. Magnetic field strength around sample installing area.

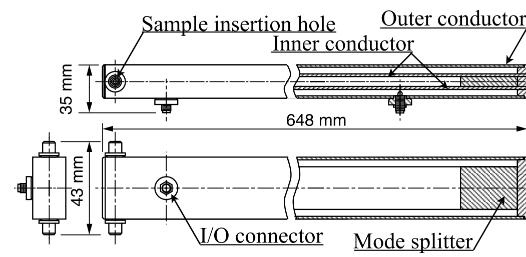

Fig. 7. Example of UHF band resonator (the longer side of the resonator is cut away to show whole).

The magnetic characteristics of materials have very strong frequency dependence from 100 MHz to 10 GHz because the relaxation frequencies of the permeability are usually found in this frequency range. Therefore, the accurate measurement of the permeability is essential in order to use the magnetic materials in this frequency range, and a seamless frequency evaluation of the material constant from 1 to 2 GHz is essential. However, the expansion of the frequency range to the UHF range requires a huge size of the waveguide, and the frequency range of the waveguide resonator becomes narrow.

The use of a TEM-mode transmission line resonator was considered for the evaluation of the permeability at the UHF range because the line has no cutoff frequency. The minimum resonance frequency is defined only by the length of the line, and the line resonates at the integer multiples of the lowest resonance frequency. The lowest resonance frequency of 250 MHz was selected considering the length of the resonator and the number of the resonance frequencies to S-band, 2 GHz. The magnetic flux density for the both ends of the sample should be null for the seamless connection of the results obtained at the higher frequency. The odd modes in the coaxial line with two parallel center conductors were considered. The structure of the test fixture is shown in Fig. 7, as an example. When each line is driven by the same magnetic field strength and the reverse-phase angle, the magnetic flux of the odd mode appears at the center of the parallel line, and the magnetic flux distribution would satisfy the requirement described above. However, in actual cases, significantly, the even mode appears even if the driving condition described above were maintained. Therefore a mode splitter at one end of the center conductor was provided to distinctly separate the even and the odd resonance modes.

The magnetic field strength of the UHF band cavity around the sample installing area is shown in Fig. 8.

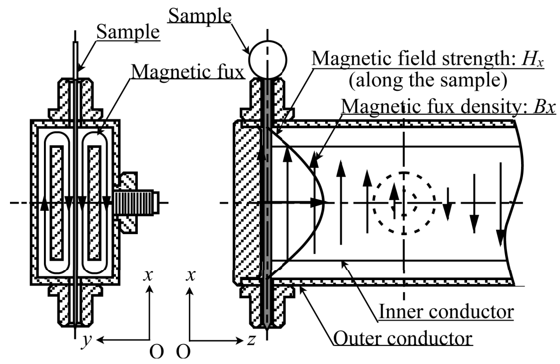

Fig. 8. Example of UHF band resonator.

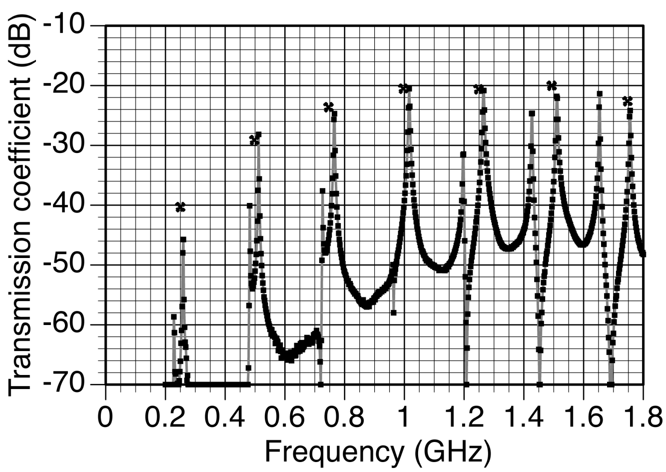

Fig. 9. Simulated result of UHF resonator.

Fig. 8 shows that the magnetic field strength H_x,, at the center of the sample area is the maximum and 0 at the top and the bottom of the cavity, as shown in Fig. 8. This means the demagnetization field is 0 at both ends of the sample.

The electromagnetic simulation was carried out to optimize the position of the driving and the detecting loop antennas of the resonator with the mode splitter. An example of the transmission characteristics for the odd modes resonator, given by the simulation, is shown in Fig. 8. The simulation results were given with the two modes, and the resonance peaks of the odd mode are indicated by asterisks.

The results in Fig. 9 show that the resonance peak values of the even mode at higher frequency range are high, and the separation of the even mode from the odd mode looks not good enough. Methods to solve the problems will be discussed in the next section.

B. Design and Assemble of Harmonic Resonators

The resonance frequency range of the measuring system is separated into five bands. The lengths of the resonators were defined to have seven or eight resonance frequencies, as shown in Table I. The results obtained by the structure simulations are used to define the driving and the detecting loop antenna positions of the cavity.

TABLE I
SPECIFICATIONS OF HARMONIC RESONANCE CAVITY

Band	UHF	S	C	X	Ku
Housing	WR-159	WR-340	WR-159	WR-90	WR-75
Frequency (GHz)	0.25 - 1.8	1.8 - 3.6	3.6 - 7.2	7.2 - 12	12 - 18
Cavity Length (mm)	635	454	404	328	284
Measuring Points for μ	7	8	8	8	8
Insertion hole Diameter (mm)	3	3	3	3	2

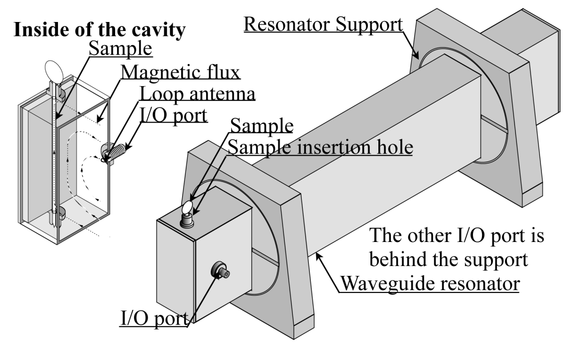

Fig. 10. Example of harmonic resonance cavity for S-band.

A cavity for S-band is shown in Fig. 10, as an example. A pair of I/O ports with loop antennas is provided at the center of the wider face of the cavity. The detailed structure of the cavity to show the relationship between the sample and the magnetic flux is also seen in Fig. 10, as the inside of the cavity. Although the magnetic flux distributes uniformly for the width of the cavity, only the flux at the center of the cavity is illustrated. The uniaxial magnetic flux generated from this loop antenna at the broad side center of the cavity could suppress the generation and the detection of TE_{20} mode observed at the higher edge of the band, and contribute to extend the operating frequency range. The line length of a grounded loop antenna should be less than a half wavelength of the highest resonance frequency because the grounded line should work as an inductor within the band. The distance between the loop antenna and the shorted end of the cavity was given by the structure simulation, as discussed earlier. The sample insertion hole consists of a pair of circular waveguides with a very high cutoff frequency throughout the measuring frequency range. The diameter of the sample insertion hole was defined, considering that the same sample could be used for wider frequency bands. The diameters of the hole are 3 mm for UHF to X-band. The diameter for the Ku band is reduced to 2 mm, considering the cutoff frequency of the hole and the cavity size. All parts of the cavity were soldered to obtain high Q-factors. The assembled cavities were tuned to obtain the transmission characteristics given by the structure simulation.

The transmission coefficients of the assembled cavities have shown good agreement to the simulation results. The result of the C-band cavity is shown in Fig. 11 as an example with the result given by the simulation. The increase of the transmission

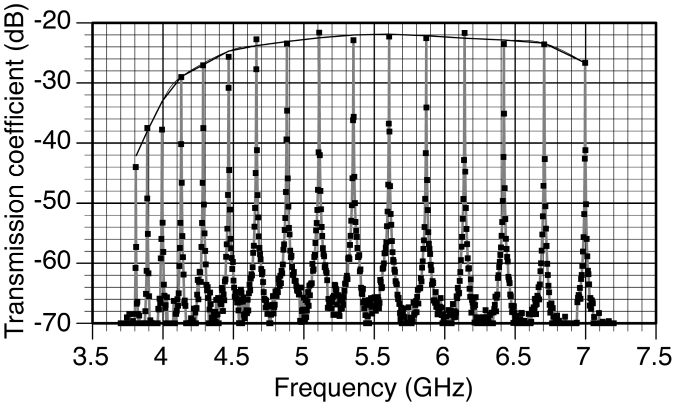

Fig. 11. Comparison of the actual results and the simulation (peak value given by the simulation is shown as a dotted line).

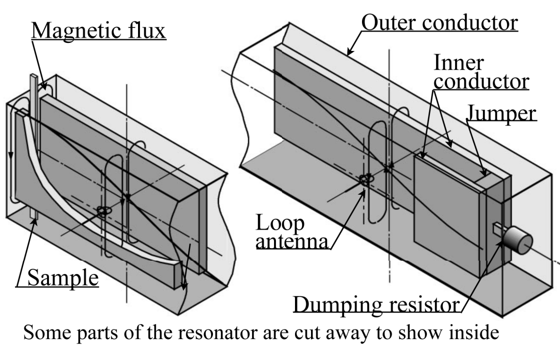

Fig. 12. Improved structure of UHF transmission line resonator.

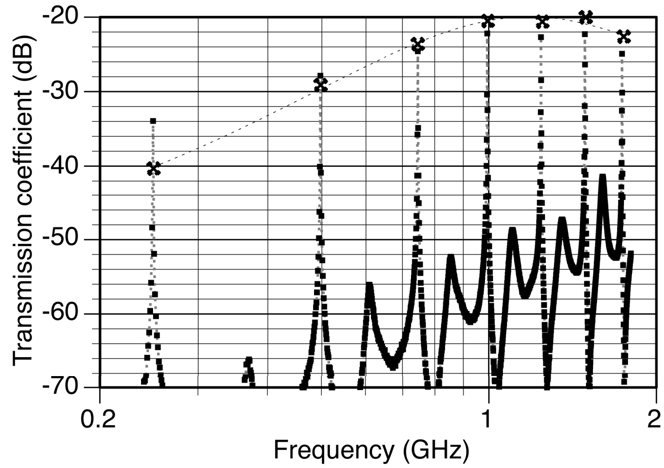

Fig. 13. Comparison of the actual results and the simulation.

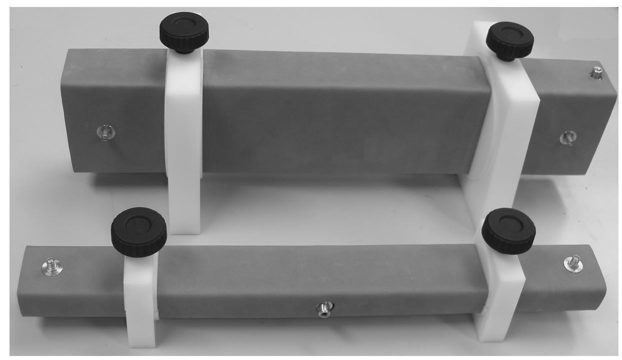

Fig. 14. Assembled cavities for *S*-band (top) and *C*-band (bottom).

coefficient with the frequency was suppressed by defining the position of the loop antenna, as given by the simulation described earlier.

For the evaluation of the permeability of the anisotropic materials in the UHF band, there needs to be sufficient separation of the odd and the even modes. However, the measurements of the anisotropic materials at the UHF and the *S*-band have shown a clear gap at the two frequency bands. The difficulty of driving the resonator by the complex conjugate signals was the main reason for the gap, and therefore, a more advanced structure to suppress the even mode was required. An improved structure, as shown in Fig. 12, was finally selected.

This structure could be called a flattened ring resonator. The equal current throughout the inner conductors creates the same magnetic flux around the sample, as shown in Fig. 10, and this profile satisfies the magnetic flux distribution requirement described above. Although the flattened ring resonator generates the same magnetic flux distribution as the odd mode, the resonator has the other resonance frequencies corresponding to when the inner conductor length is equal to the odd number multiples of the quarter-wavelength of the resonance frequencies. The magnetic flux distribution is very close to the even mode described above except that this resonator is open ended. This means that at the open end, the electric field strength is the maximum and the magnetic field strength is zero at the open end. The unfavorable modes were suppressed by connecting a resistor between the open end and the outer conductor, as shown in Fig. 12.

The transmission coefficient of the improved resonator is shown in Fig. 13 with the resonance peak value obtained from the structure simulation. The actual result and the simulation result have given a good agreement, as shown in Fig. 13. The results also show the unfavorable modes that were sufficiently suppressed.

C. Assembled Cavity Resonators

Four waveguide resonators for *S*-, *C*-, *X*-, and Ku-bands and one coaxial line resonator for the UHF band were assembled. The resonators for *S*- and *C*-bands are shown in Fig. 14 as examples.

It is convenient to install the samples vertical in the resonator. Therefore the resonators are supported by a rotatable stage for the evaluation of permittivity in the future using samples inserted in holes through the orthogonal surface of the cavity. The cavity temperature change causes the resonance frequency change, -15 ppm/°C, and this change decreases the accuracy of the permeability evaluation. Therefore the cavities are covered by thermal insulating material, foamed polyethylene sheet to prevent the rapid change of the cavity temperature.

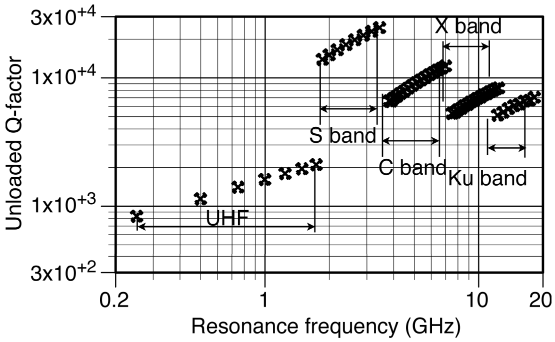

Fig. 15. Examples of assembled cavity characteristics.

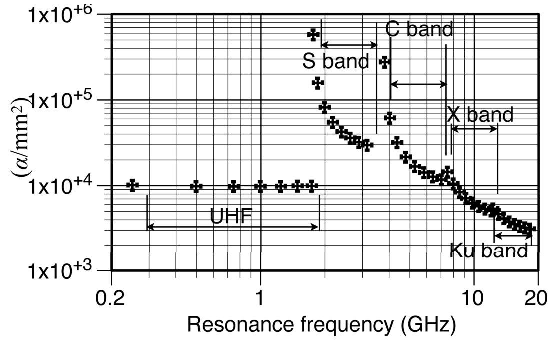

Fig. 16. Examples of α_{m}.

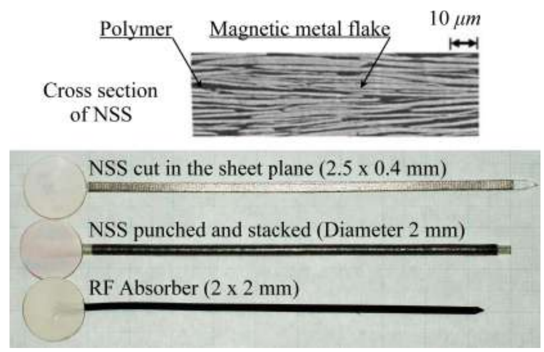

Fig. 17. Cross section of NSS and samples used in the measurement.

The Q-factor of the cavities in terms of the resonance frequencies for each band are shown in Fig. 15 as examples.

III. Permeability Evaluation

The NRW method has been widely used in the frequency-dependent permeability of materials in the microwave frequency range. The comparison of the NRW method and the HRCP method will be made in this section. The evaluation method using a shorted transmission line was not considered here because the adjustment of the demagnetization effect would be complicated. In the HRCP method, the sample is installed in the insertion hole of the cavity provided where only the magnetic field is found, as shown in Fig. 2. Fig. 2 shows that the magnetic field is applied along the long axis of the sample (x-axis), and the magnetic field strength at both ends of the sample in the cavity is null. This means that no demagnetizing field is found in the sample. The permeability obtained from the HRCP method is intrinsic and no adjustment is required. This is a big advantage of the permeability evaluation by the TE_{10n} mode rectangular waveguide cavity.

A. Calibration of Test Fixture

The definition of the proportional constant α_m in (4) should be defined first as the calibration of the test fixture. The value could be defined theoretically by substituting the shape of the sample into (1). However, the estimation of the electromagnetic volume of the cavity from the physical size was quite difficult. The constant was defined experimentally using the characteristic that the permeability of a good conductor is 0 in the microwave frequency [6]. The procedure to define α_m is shown as follows. The equation will be written in the following when the good conductor is installed in the cavity:

$$\dot{\mu} = 1 + \frac{V}{\alpha_m \Delta v}\left(\frac{F_{r0}}{F_{\mathrm{rs}} - F_{r0}}\right) = 0 \tag{7}$$

where V is the volume of the cavity, Δv is the volume of the sample, α_m is the proportional constant, F_{r0} is the resonance frequency of the blank cavity, and F_{rs} is the resonance frequency of the cavity with the sample. The equation is modified, and the proportional constant is given, as shown in the following equation:

$$\frac{V}{\alpha_m} = \left(\frac{F_{r0}}{F_{\mathrm{rs}} - F_{r0}}\right)\Delta v_s \tag{8}$$

The proportional constant, as given by (8), also solved a difficulty in determining the cavity volume V.

The constants obtained by the experiments are shown in Fig. 16 as examples. The results solved the difficulties in estimating the cavity volumes, as well as the frequency-dependent characteristics of the cavities.

When the permeability of the good conductor would be null within the frequency range, the whole results obtained by the measurement are normalized by the permeability of the good conductor. This is another advantage of the permeability measurement by the cavity perturbation method.

B. Sample Preparation

The shape of the sample should be a rod with the cross section to fit the sample insertion hole, and the length of the sample should be longer than the height of the cavity. The diameter of the hole is 3 mm, and the maximum cavity height is 90 mm in this measurement. Two materials were selected for the evaluation by the HRCP method. One sample was taken from an NSS, and the other was taken from an RF absorber sheet.

The structural cross section of the NSS and the samples for the measurement are shown in Fig. 17.

The NSS is made by kneading small flakes of magnetic metal materials into plastics. The permeability of the sheet was known to be anisotropic. A fine strip was cut from the sheet to evaluate the permeability along the sheet plane. A certain backup material was required to install into the cavity because the NSS is very thin, less than 0.4 mm in thickness. A rod of the sheet to evaluate the permeability

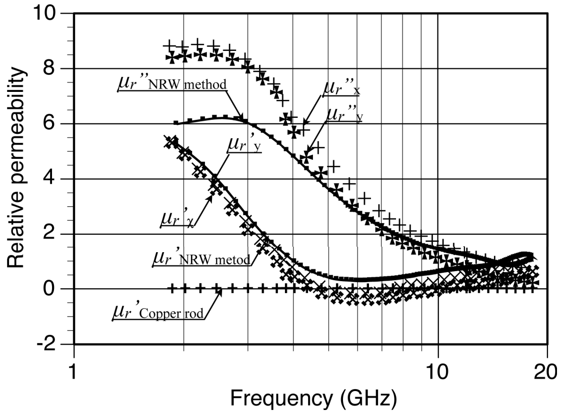

Fig. 18. Measured results comparison of HRCP and NRW methods.

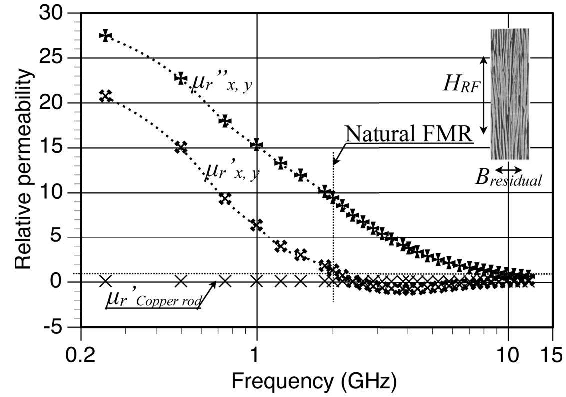

Fig. 19. Permeability of NSS plan.

along the axis perpendicular to the NSS was prepared by punching the sheet and stacking the disks. A plastic tube with the relative permeability of 1 is used to maintain the sample as a stick. Efforts to reduce the demagnetization flux on the surface of the sheets were made by stacking the unit sheet with strong pressure. Although the air gaps between the sheet reduces the permeability of the sample, the reduction would not be significant because the flakes are stacked in the polymer already, as shown in Fig. 16. A rod with a square cross section of around 2×2 mm^2 with a length of 100 mm was prepared as a sample to evaluate the permeability of the RF absorbing sheet.

C. Results of Measurement

The comparison of the results obtained by the NRW method and the HRCP method was made first as a preliminary experiment. A copper rod was prepared as a good conductor for the HRCP method to confirm the consistency of the method. The cross section of the NSS for the HRCP method was 2×0.3 mm^2, and the good conductor is 2 mm in diameter. The lengths of the samples are prepared longer than 100 mm to exceed the cavity height. A thin toroid to fit a 7-mm coaxial line was cut out from the sheet with 0.3 mm thickness for the NRW method. The measured results are shown in Fig. 18.

Significant differences between the results of the NRW method and the HRCP method were observed. The results obtained by the HRCP method showed that the permeability in the sheet plane, μ_x and μ_y, have a little difference, and the anisotropy of the permeability in the plane would not be significant. In the measurement of the copper rod, the permeability difference from 0 means the accuracy of the HRCP method. The standard deviation, σ, of the result was 0.0042. The accuracy of the HRCP method is estimated by 3σ, and 1.3% is the accuracy of the permeability evaluated by the HRCP method. The measurement of the permeability for a good conductor confirms the consistency of the measurement by the HRCP method. This is also a big advantage of the HRCP method. The reason for the difference obtained by the NRW method from the HRCP method is not clear. It could be caused by the different structures of the test fixture for the two methods. The NRW method requires that the sample should fill the space between the center conductor and the ground conductor completely. The requirement of the NRW method makes it very difficult to measure the permeability of the good conductor as the reference material. The comparison of the two results also suggests that the number of measuring points of 8 in the band is appropriate to show the profile of the material characteristics.

The permeability evaluation for all the samples shown in Fig. 17, different from the sample used in the measurement of Fig. 18, were carried out next. The results are shown in Figs. 19–21. The directions of the RF magnetic field and the residual magnetic fluxes in the sample cross section are shown in Figs. 19–21.

The permeability of NSS parallel to the sheet plane, shown in Fig. 19, was big at the lower frequency and decreased with the frequency. The decrease of the permeability as the frequency increases from 0.2 to 1 GHz would be caused by the decrease of the magnetic wall motion in the flake. Further decrease of the permeability was observed for the higher frequency and crossed at $\mu_r' = 1$ around 2 GHz. This fact shows that the natural ferromagnetic resonance is generated, and the magnetic loss hump should be observed. However, a clear magnetic loss hump is not found. It would be masked by the significant loss of the wall motion. The decrease of the permeability proceeded further to negative and came to a minimum of approximately $\mu_r' = -1$ at around 3 GHz. Then the permeability turned to increase gradually, but the value was not more than 1. The behavior of the permeability higher than 2 GHz is an aftereffect of the natural ferromagnetic resonance caused by the residual magnetization in the flake. The thin magnetic flake showed a weak orientating dc magnetic field depressed by the demagnetization at the surface of the flake. The ferromagnetic resonance at lower than 1 GHz would be masked by the permeability based on the big wall motion in the flake.

The permeability along the axis perpendicular to the sheet plane is shown in Fig. 20.

The permeability is one order smaller than the sample cut along the plane. Around the frequency of 1.5 GHz, the permeability crossed $\mu_r' = 1$, and the magnetic loss became the maximum. This is a typical appearance of the natural ferromagnetic resonance. A strong demagnetizing field

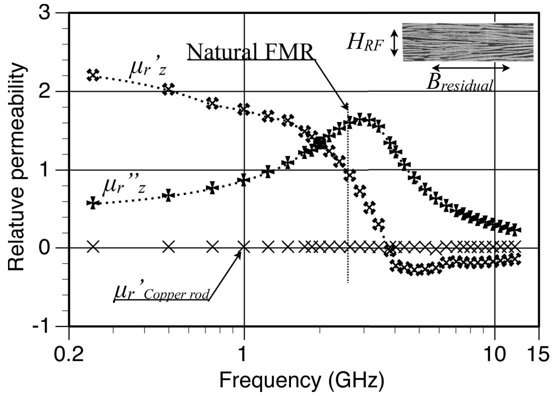

Fig. 20. Permeability of NSS along the perpendicular axis.

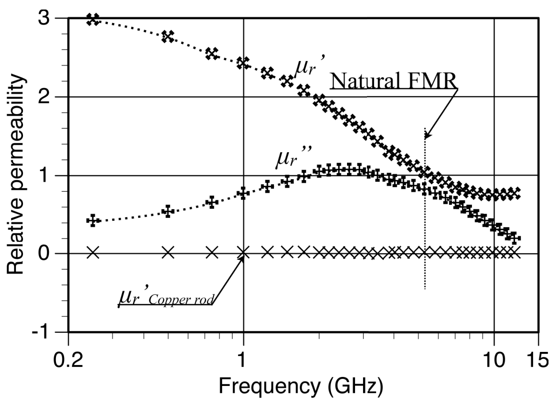

Fig. 21. Permeability of RF absorbing sheet.

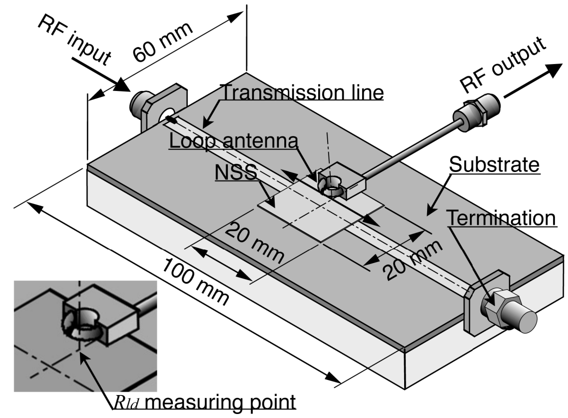

Fig. 22. Structure of line decoupling ratio measuring apparatus.

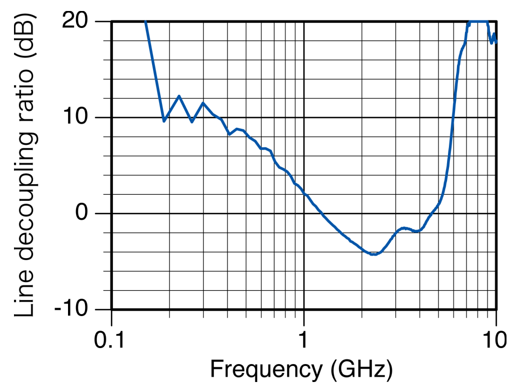

Fig. 23. Line decoupling ratio of NSS.

restricted the motion of the spin in the RF field, and a weak demagnetizing field at both ends of the flake increased the residual magnetic field in the flake. The two terms described above explain the smaller permeability and the higher resonance frequency of this sample.

The permeability of a sample taken from an RF absorbing sheet is shown in Fig. 21. The permeability of the good conductor in the results means the measured permeability of the RF absorber is consistent.

The simple decrease of μ_{r}' with the increase of the frequency was observed. The loss factor $\mu_{\mathrm{r}}^{\gg}$ made a small peak around 2 GHz. This would be the Debye type relaxation process by the magnetic wall motion. A small hump of the magnetic loss observed at the frequency that μ_{r}' crossing 1, around 5 GHz, suggests that the natural ferromagnetic resonance would be generated partially in the sample.

D. Confirmation by Experiments

Although the negative permeability of NSS was understood by the effect of the natural ferromagnetic resonance, the results obtained by the HRCP method were very unusual. The confirmation of the negative permeability in the actual circuit was carried out by using an apparatus to evaluate the line decoupling ratio (R_{ld}) defined in the document IEC 62333-2 [13]. The structure of the test fixture is shown in Fig. 22.

The loop antenna to detect the magnetic flux from the line is fixed at the center of the NSS, as shown in Fig. 22. The R_{ld} is the ratio of the RF output power from the transmission line and the power after the NSS is installed. The results obtained by the NSS shown in Fig. 17 is shown in Fig. 23. The negative value in dB of the R_{ld} means that the RF power detected by the loop antenna was increased by installing the NSS.

In the actual measurement, the loop antenna was moved parallel to the transmission line to detect the magnetic flux density distribution along the line. The measured magnetic flux density is shown in Fig. 24.

The magnetic flux density in Fig. 24 was normalized by the flux density at the measuring position in Fig. 24, and the inverse of the flux density corresponds to R_{ld}. As is seen in Fig. 19, the relative permeability of the NSS was more than 1 at lower than 2 GHz, and the value became less than 1 at higher than the frequency. At lower than 2 GHz, the relative magnetic flux density is lower than 1 on the NSS. This suggests that this magnetic flux penetrates into the NSS, and the flux density outside of the sheet is reduced. At frequencies higher than 2 GHz, the permeability of the NSS decreased from 1, and the sheet repels the magnetic flux. The repelled magnetic flux turns to the loop antenna, and the measured flux density was increased. It was confirmed that the permeability less than 1 actually occurs.

A small ripple observed in Fig. 24 typically found at 2.5 GHz suggests a weak standing wave is generated in the NSS. The ripple could be caused by the high permittivity of the NSS. The effective permittivity of the NSS can be

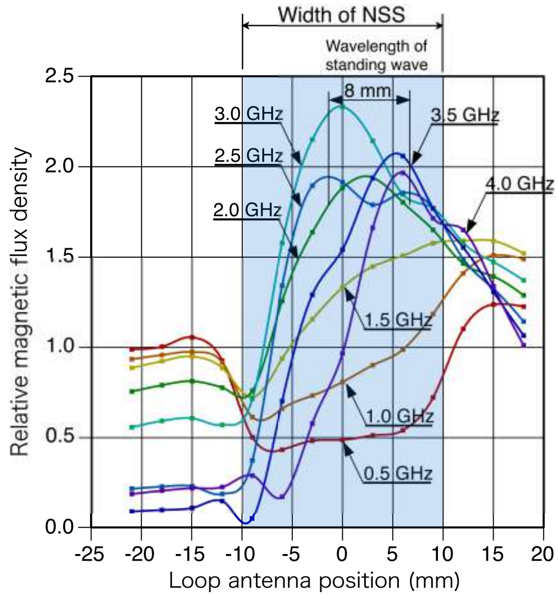

Fig. 24. Magnetic flux density of NSS along the transmission line.

estimated by comparing the wavelength of the standing wave, approximately 8 mm in Fig. 24 at a wavelength of 2.5 GHz. The relative permittivity of NSS, $\varepsilon_{\mathrm{r\_eff}}$, was estimated by

$$\sqrt{\varepsilon_{\mathrm{r\_eff}}} = \frac{\lambda_0}{\lambda_{\mathrm{NSS}}} \tag{9}$$

where λ_0 is the wavelength in the free space and λ_{NSS} is the wavelength in the NSS. The estimated relative permittivity of 225 suggests the NSS structure shown in Fig. 17 has high permittivity along the plane of the sheet.

As discussed in this section, the permeability less than 1 actually occurs. The frequency-dependent permeability evaluation for broadband without the depolarization and the evaluation of anisotropic characteristics of the material with the permeability of the good conductor have shown the great advantage of the HRCP method. This is the first evaluation of the frequency-dependent permeability by the HRCP method.

ACKNOWLEDGMENT

The authors would like to appreciate the stimulating discussions and the invaluable advice of Prof. L. E. Davis of the University of Manchester, Manchester, U.K., to complete this article. This work was started to draft the IEC standard 62333 “Noise Suppression Sheet for Digital Device and Elements.” The authors express their deep thanks to the encouragements and the supports of the IEC/TC51/WG10 Japanese Committee Members. The authors also acknowledge with the contribution of Dr. M. Horibe and Mr. Y. Kato of the National Institute of Advanced Industrial Science and Technology.

REFERENCES

[1] A. M. Nicolson and G. F. Ross, “Measurement of the intrinsic properties of materials by time-domain techniques,” *IEEE Trans. Instrum. Meas.*, vol. IM-19, no. 4, pp. 377–382, Nov. 1970.

[2] W. B. Weir, “Automatic measurement of complex dielectric constant and permeability at microwave frequencies,” *Proc. IEEE*, vol. 62, no. 1, pp. 33–36, Jan. 1974.

[3] V. Bekker, K. Seemann, and H. Leiste, “A new strip line broad-band measurement evaluation for determining the complex permeability of thin ferromagnetic films,” *J. Magn. Magn. Mater.*, vol. 270, no. 3, pp. 327–332, Apr. 2004.

[4] S. Takeda, S. Motomura, T. Hotchi, and H. Suzuki, “Permeability measurement system up to 10 GHz using all shielded shorted microstrip line,” *J. Jpn. Soc. Powder Powder Metall.*, vol. 61, no. S1, pp. S303–S307, 2014.

[5] A. Vepsalainen, K. Chalapat, and G. S. Paraoanu, “Measuring the microwave magnetic permeability of small samples using the short-circuit transmission line method,” *IEEE Trans. Instrum. Meas.*, vol. 62, no. 9, pp. 2503–2510, Sep. 2013.

[6] B. Lax and K. Button, *Microwave Ferrites and Ferrimagnetics*. New York, NY, USA: McGraw-Hill, 1962, pp. 330–335.

[7] N. Ogasawara, “On the measurement of permittivity and tensor permeability of thin rods of ferrites,” (in Japanese), *J. Inst. Elect. Eng. Jpn.*, vol. 77, no. 825, pp. 1–6, 1957.

[8] R. A. Waldron, “Perturbation theory of resonant cavities,” *Proc. IEE C, Monographs*, vol. 107, no. 12, p. 272, Sep. 1960.

[9] A. Kumar, “Measurement of permittivity of materials at microwave frequency: A review,” in *Proc. 19th Electr. Electron. Insul. Conf.*, 1989, pp. 73–77.

[10] S. Sharma, A. Kumar, and D. Kaur, “Cavity perturbation measurement of complex permittivity of dielctric material at microwave frequencies,” *Int. Jour. Emer. Tech. Comp. Appl. Sci.*, vol. 4, no. 1, pp. 116–120, 2013.

[11] T. Miura, K. Tahara, and M. Horibe, “Evaluation of frequency-depend permeability by harmonic resonance cavity perturbation method,” in *Proc. Asia–Pacific Microw. Conf.*, Sendai, Japan, 2014, pp. 513–515.

[12] T. Miura, “A proposal for standard to compare Q-factor evaluation accuracy of microwave resonator,” in *IEEE MTT-S Int. Microw. Symp. Dig.*, Jun. 2006, pp. 1963–1966.

[13] *Noise Suppression Sheet for Digital Devices and Equipment—Part 2: Measuring Methods*, Standard IEC 62333-2, 2006, pp. 24–27.

Taro Miura (Life Member, IEEE) received the B.E. degree in electrical engineering from Keio University, Tokyo, Japan, in 1962, and the D.E. degree in electronic engineering from the Tokyo Institute of Polytechnic, Tokyo, in 1996.

From 1962 to 1998, he was with TDK Corporation, Tokyo. He has mainly been engaged in the development and evaluation of RF passive devices using ferrite and dielectric materials. From 1998 to 2002, he was the President and a Manager of technical support with TDK Techno Corporation. From 2004 to 2007, he was a Senior Visiting Research Fellow with the University of Manchester, Manchester, U.K., where he is involved in the study of microwave ferrite nonlinearity. In 2008, he started to work as a consultant of RF materials characterization.

Dr. Miura is a member of the Institute of Electronics, Communication and Information Engineering (IEICE), Japan, and the IEEE Microwave Theory and Techniques Society (IEEE MTT-S).

Ken Tahara (Member, IEEE) received the B.E. degree in electrical engineering from Kogakuin University, Tokyo, Japan, in 1964.

From 1958 to 1972, he was with the NTT Electronic Engineering Laboratory. From 1972 to 1982, he was with Hitachi Electronic Corporation. In 1982, he founded Kanto Electronics Application and Development Corporation to develop the mm-wave components, the bulk oscillators, and detectors, where he has been the President until 2019. He is currently with KEN-TEK Corporation, Tokyo.

Mr. Tahara is a member of the Institute of Electronics, Communication and Information Engineering (IEICE), Japan, and the IEEE Microwave Theory and Techniques Society (IEEE MTT-S).